

Cooperation Based Joint Active and Passive Sensing with Asynchronous Transceivers for Perceptive Mobile Networks

Wangjun Jiang, *Student Member, IEEE*, Zhiqing Wei, *Member, IEEE*,
 Shaoshi Yang, *Senior Member, IEEE*, Zhiyong Feng, *Senior Member, IEEE*,
 Ping Zhang, *Fellow, IEEE*

Abstract

Perceptive mobile network (PMN) is an emerging concept for next-generation wireless networks capable of conducting integrated sensing and communication (ISAC). A major challenge for realizing high performance sensing in PMNs is how to deal with spatially separated asynchronous transceivers. Asynchronicity results in timing offsets (TOs) and carrier frequency offsets (CFOs), which further cause ambiguity in ranging and velocity sensing. Most existing algorithms mitigate TOs and CFOs based on the line-of-sight (LOS) propagation path between sensing transceivers. However, LOS paths may not exist in realistic scenarios. In this paper, we propose a cooperation based joint active and passive sensing scheme for the non-LOS (NLOS) scenarios having asynchronous transceivers. This scheme relies on the cross-correlation cooperative sensing (CCCS) algorithm, which regards active sensing as a reference and mitigates TOs and CFOs by correlating active and passive sensing information. Another major challenge for realizing high performance sensing in PMNs is how to realize high accuracy angle-of-arrival (AoA)

This work is supported in part by the National Key Research and Development Program under Grant 2020YFA0711302, in part by the Beijing Municipal Natural Science Foundation under Grant L202012 and Grant Z220004, in part by the Fundamental Research Funds for the Central Universities under Grant 2020RC05, and in part by the BUPT Excellent Ph.D. Students Foundation under Grant CX2022207. *Corresponding author: Zhiyong Feng and Zhiqing Wei.*

W. Jiang, Z. Wei, S. Yang and Z. Feng are with the School of Information and Communication Engineering, Beijing University of Posts and Telecommunications, and also with the Key Laboratory of Universal Wireless Communications, Ministry of Education, Beijing 100876, China (email: {jiangwangjun, weizhiqing, shaoshi.yang, fengzy}@bupt.edu.cn).

P. Zhang is with the School of Information and Communication Engineering, Beijing University of Posts and Telecommunications, and also with the State Key Laboratory of Networking and Switching Technology, Beijing 100876, China (email: pzhang@bupt.edu.cn).

estimation with low complexity. Correspondingly, we propose a low complexity AoA algorithm based on cooperative sensing, which comprises coarse AoA estimation and fine AoA estimation. Analytical and numerical simulation results verify the performance advantages of the proposed CCCS algorithm and the low complexity AoA estimation algorithm.

Index Terms

Joint active and passive sensing, cooperative sensing, integrated sensing and communication (ISAC), angle-of-arrival (AoA), timing offset (TO), carrier frequency offset (CFO).

I. INTRODUCTION

A. Background and Motivation

Perceptive mobile network (PMN) [1], [2] is an emerging concept for next-generation wireless networks that combine sensing and communication capabilities (ISAC) to serve as a ubiquitous environment sensing network while maintaining reliable mobile communication services [3]. In [4], Zhang *et al.* conducted an in-depth study on the capability of sensing the user equipment (UE) by the sensing base station (SBS) in PMN, and defined three types of sensing: downlink active sensing, downlink passive sensing, and uplink passive sensing. In a PMN, active sensing and passive sensing may co-exist [4]. For active sensing, the transmitter and receiver are co-located, which means that they can be conveniently synchronized at the clock level [5], [6]. However, for passive sensing, the transmitter and receiver are spatially separated and asynchronous, which results in timing offsets (TOs) and carrier frequency offsets (CFOs), thus leading to degradation of sensing accuracy with respect to ranging and velocity measurements.

To obtain high performance sensing in a PMN, joint active and passive sensing is advocated as a promising technique [7], where cooperation between co-existing active sensing and passive sensing is exploited. A major challenge facing cooperation based joint active and passive sensing is how to achieve high performance passive sensing with spatially separated asynchronous transceivers. On the one hand, most existing passive or cooperative sensing algorithms assumed perfect synchronization between receivers and transmitters, and did not consider the influence of TOs and CFOs on the cooperative sensing performance [8]–[10]. On the other hand, a few contributions resort to mitigate TOs and CFOs based on the line-of-sight (LOS) path between the sensing-oriented receiver and transmitter, but the LOS path may not exist in realistic scenarios

[11], [12]. For a PMN operating in the non-LOS (NLOS) environment, mitigating the TOs and CFOs in passive sensing remains an open problem that has to be solved.

Since the scale of antenna arrays deployed on SBS is limited, how to achieve high accuracy angle-of-arrival (AoA) estimation with limited-size antenna arrays is another challenge facing the cooperation based joint active and passive sensing. Most existing algorithms [12]–[15] use both time-domain and spatial-domain measurements to improve the accuracy of AoA estimation, but the computational complexity is excessively high. Therefore, how to realize high accuracy AoA estimation with low complexity in the context of PMN is also an important problem that needs to be solved.

B. Related Work

There have been some related studies that are valuable for solving the above mentioned challenges confronting the cooperative sensing in PMN. The major state-of-the-art contributions are described as follows.

1) TO and CFO mitigation in the presence of asynchronicity:

In wireless communications, some efforts have been devoted to the asynchronicity problem in cognitive radio [16]–[18]. However, these studies focused on the analysis of interference caused by asynchronicity, such as the inter-symbol interference (ISI) and inter-carrier interference (ICI) caused by TOs and CFOs [19], [20], without providing effective methods for parameter estimation.

In wireless sensing, TO and CFO can directly cause timing and Doppler estimation ambiguity and hence leading to degradation of sensing accuracy with respect to ranging and velocity measurements. Existing synchronization algorithms for sensing can be divided into three categories: GPS clock, and single-node-based and network-based solutions [21].

- GPS clock synchronization is suitable for outdoor environments that can receive GPS signals. The synchronization accuracy of GPS-assisted synchronization is sufficient for communications, but not for target sensing. For example, for a typical GPS clock stability error of 20 ns, this translates into a ranging error of 6 m.
- Single-node-based synchronization can be implemented in a single receiver. The cross-antenna cross-correlation (CACC) method is a typical single-node-based synchronization algorithm, which is widely used in Wi-Fi sensing [22]–[24]. However, the CACC method

mitigate TOs and CFOs based on the assumption that there is a strong LOS path between the sensing receiver and transmitter, which may not be suitable in NLOS scenarios.

- Network-based synchronization exploits measurements from multiple cooperative nodes. One of the typical network-based synchronization method is the trilateration, which exploit known geometric relationships to remove TO and CFO [25]. Other techniques deal with asynchrony by taking advantage of the statistical averaging effect of multiple measurements. However, the above methods have the problems of high complexity and difficult multi-target association, which could be concerns for real-time implementation.

2) *AoA estimation for wireless sensing*: Another major challenge for realizing high performance sensing in PMNs is how to accurately estimate the AoA of the target. AoA estimation algorithms based on the combination of multiple-domain information are proposed in [12]–[14]. More specifically, Ni *et al.* [12] attempt to equivalently extend the length of the spatial array response vector by integrating the time and frequency domain signals into the spatial domain, thereby obtaining higher accuracy in AoA estimation. In [13], Chuang *et al.* jointly combine spatial and temporal domain information to obtain high-accuracy AoA estimation. In [14], Ni *et al.* define a spatial path filter to separate signals sent over multiple propagation paths and obtain AoA through the CACC output. However, the above three algorithms that improve the accuracy of AoA estimation by expanding the length of the spatial array response vector lead to a substantial increase in the computational complexity.

C. Main Contributions of Our Work

Against the above backdrop, we propose a cooperation based joint active and passive sensing scheme for improving the performance of SBS in a PMN that experiences the NLOS propagation, and our focus is on overcoming the asynchronicity problem in passive sensing and the low-complexity high-accuracy AoA estimation challenge with limited scale of antenna arrays. Our major contributions are summarized as follows.

- 1) Considering NLOS propagation, we provide a cooperation based joint active and passive sensing scheme that does not require clock-level synchronization between the spatially separated and asynchronous transceivers. Simulation results show that when the power of the active echo signal is close to that of the passive echo signal, the performance of cooperative sensing becomes appreciably superior to both the active sensing and passive sensing.

- 2) Considering the single target estimation scenario, we propose a cross-correlation cooperative sensing (CCCS) method that regards active sensing as a reference and mitigates TOs and CFOs existing in passive sensing by correlating active and passive sensing information. Compared with CACC proposed in [12], CCCS is more widely applicable, because it does not require the existence of LOS propagation paths between transceivers.
- 3) Considering the multiple-target estimation scenario, we propose a multi-target alignment algorithm to handle the outputs of the CCCS method, so that the problem of inter-target correlation interference can be solved. Compared with the single target scenario, it is more challenging to estimate TOs and CFOs in the multi-target scenario by directly using CCCS, because in this situation the outputs of CCCS not only contain information on TOs and CFOs of the same target, but also contain information on the delay and Doppler spread correlation between different targets. This correlation may hamper the subsequent TOs and CFOs mitigation operations. The multi-target alignment algorithm includes two stages, i.e., the extraction stage and the matching stage. In the extraction stage, TOs and CFOs of the same target can be extracted with the aid of spatial information differences of different targets. Then TOs and CFOs of different targets are matched in the matching stage, as detailed in Section III-C2. Simulation results demonstrate that the multi-target alignment algorithm works well when the variance of CFOs is smaller than $\frac{1}{4}$ of the subcarrier spacing, which can be satisfied by ordinary frequency sources [26]–[28].
- 4) We develop a low-complexity high-accuracy AoA estimation algorithm based on cooperative sensing and fractional Fourier transform (FRFT). Although traditional FRFT can significantly improve the accuracy of AoA estimation, its way of expanding the number of Fourier transform points increases its computational complexity [29]. To reduce the complexity while ensuring high-accuracy AoA estimation, we propose an AoA estimation algorithm relying on iterations between coarse estimation and fine estimation. In the coarse estimation stage, we obtain a rough AoA result of targets by cooperative active and passive sensing. In the fine estimation stage, we further obtain a fine AoA of targets by the FRFT algorithm within the range of the rough AoA result. We analyze and simulate the accuracy and complexity of different AoA estimation algorithms, including the hybrid multiple signal classification (H-MUSIC) [13], hybrid estimation of signal parameters via rotational invariance techniques (H-ESPRIT) [13], joint time-space-frequency (TSF) domain MUSIC algorithm (TSF-MUSIC) [12], and FRFT [29]. simulation results show

that the AoA algorithm proposed in this paper can achieve relatively high-performance AoA estimation, close to FRFT, at a low complexity, much lower than FRFT.

The rest of this paper is organized as follows. In Section II we describe the system model of the cooperation based joint active and passive sensing. The cooperative sensing for delay and Doppler spread is introduced in Section III. In Section IV we present the proposed low-complexity high-accuracy AoA estimation algorithm. Range, velocity and AoA estimation are analyzed and numerically evaluated in Section V. Finally, Section VI concludes the paper.

Notations: Vectors and matrices are denoted by boldface lowercase and uppercase letters; the transpose, complex conjugate, Hermitian, inverse, and pseudo-inverse of the matrix \mathbf{A} are denoted by \mathbf{A}^T , \mathbf{A}^* , \mathbf{A}^H , \mathbf{A}^{-1} and \mathbf{A}^\dagger , respectively; $\text{diag}(\mathbf{x})$ denotes a diagonal matrix whose diagonal elements are the elements of \mathbf{x} ; $\mathcal{S}(x_i)$ denotes the set of x_i ; \otimes represents the Kronecker product; \odot denotes the Hadamard product.

II. SYSTEM MODEL OF COOPERATIVE SENSING

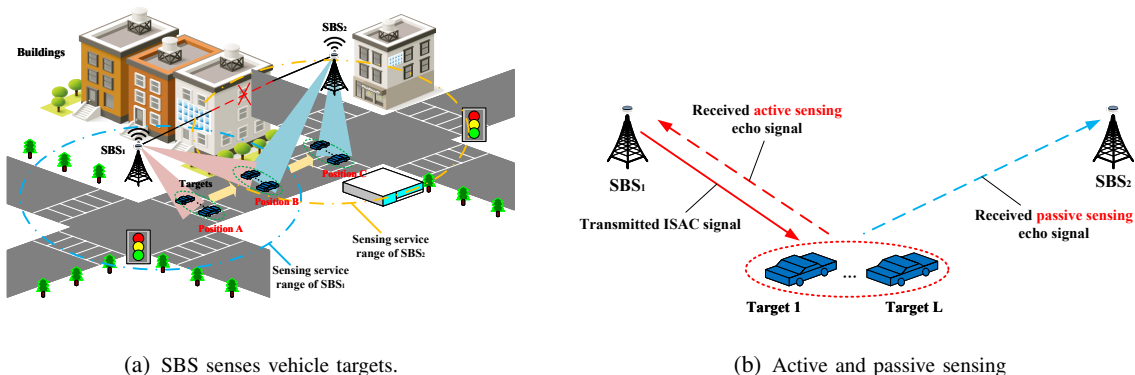


Fig. 1: System model of cooperative sensing.

We consider the cooperation based joint active and passive sensing in a PMN. As Fig. 1 shows there is no LOS propagation path between SBS₁ and SBS₂ due to the occlusion of buildings. Each SBS with N_t antennas, transmits ISAC signal to targets. These targets are not only sensing targets but also communication users. On the one hand, these targets obtain communication services by demodulating ISAC signals sent from SBS. On the other hand, SBS can receive the echo signal reflected by targets to realize the target sensing. These targets move along the road, across the sensing service range of SBS₁ and SBS₂. To provide continuous and high-performance sensing services for these targets, we propose a collaboration scheme between SBS₁ and SBS₂.

It should be noted that, in this paper, we focus on the use of ISAC technology to empower conventional communication base stations with sensing capabilities.

- In terms of signal design, we just reuse the OFDM communication signals of the existing base stations to achieve sensing without modification, and therefore, there is no significant interference to the communication performance.
- In terms of communication interaction, we just use the echo signal reflected from the base station after the target for active and passive sensing, without destroying the original communication link, therefore, there is no obvious interference to the communication performance. Compared to the traditional communication base station, one of the biggest differences is that the ISAC base station needs to deploy two antenna arrays to simultaneously complete the ISAC signal transmission and echo signal reception. This can be done by increasing the cost of hardware to mitigate the degradation of communication performance.

Therefore, we think that the reduction in communication performance can be compensated by the use of appropriate technology and hardware cost inputs, and in this paper we do not focus on analyzing the specific performance of the communication link. There have been related studies on how to design ISAC waveforms to trade-off sensing and communication performance [30], which is not the focus of this paper and may be further investigated in future work.

A. Cooperation between SBS_1 and SBS_2

As Fig. 1(a) shows, when targets are in position A, in the sensing service range of SBS_1 , SBS_1 can provide active sensing services for targets; when targets are in position C, in the sensing service range of SBS_2 , SBS_2 can provide active sensing services for targets. However, when targets are in position B, in the sensing service overlap range of SBS_1 and SBS_2 , the power of active sensing echo signal is weak, making it difficult for SBS_1 and SBS_2 to provide high-performance active sensing services for targets. We first use passive sensing to make up for the lack of performance of active sensing. However, the transceiver nodes of passive sensing are spatially separated asynchronously, resulting in TOs and CFOs, which further cause ambiguity in ranging and velocity sensing. To solve the above problem, we provide a cooperation based joint active and passive sensing scheme, including the following steps:

- Parameter setting: SBS_1 and SBS_2 adopt different signal parameters to distinguish the received active and passive sensing echo signals, as shown in Fig. 1(b). The techniques

for separating echo signals of adjacent base stations are relatively mature, including time division (TD) scheme, frequency division (FD) scheme, code division (CD) scheme, etc. Although it is easier to distinguish between active and passive sensing signals in the TD scheme, active and passive sensing of the target cannot be simultaneously achieved by the SBS in this case [31]–[33]. By contrast, in the CD scheme, SBS can achieve active and passive sensing of the target at the same time, but it requires complex coding design and signal processing to distinguish between active and passive sensing signals [30], [34]. In this paper, under the condition of sufficient spectrum resources, we assume that adjacent SBSs adopt the FD scheme [35], which is widely adopted for adjacent base stations in the 4-th generation (4G) and the 5-th generation (5G) mobile communication systems [36].

- Initiation of cooperative sensing: When SBS₁ receives the echo signal sent from SBS₂, SBS₁ will send a cooperative sensing request to SBS₂. After receiving the reply of SBS₂, the two SBSs will start cooperative sensing at the same time to generate a sensing beam pointing to the target area.
- Signal processing of cooperative sensing: When SBS₁ receives the active and passive sensing echo signals, it will perform cooperative sensing based on CCCS, which will be described in detail in Section III.

B. Received Signal Model of SBS

SBSs in a PMN can provide both sensing and communication services to UEs by transmitting ISAC signals. In the ISAC system, ISAC base stations not only need to improve sensing services, but also need to provide communication services for communication users. If the conventional sensing waveforms are used, it is difficult to guarantee the performance of the communication link. Therefore, the orthogonal frequency division multiplexing (OFDM) signal was used for joint sensing and communication [37]. In terms of communication, OFDM signal is the waveform of the 4G and 5G mobile communication systems, hence it not only has advantages in mitigating multipath interference and exploiting frequency diversity, but also enjoys standard compatibility [38]. In terms of sensing, OFDM signal has advantages in accuracy, resolution and flexibility [39]. The number and the spacing of subcarriers can be adjusted flexibly to obtain the ambiguity function of “pushpin shape” [40]. Therefore, OFDM signal is adopted as the sensing waveform

of the SBS in this paper. Then, the received signal of SBS₁ can be expressed as

$$y(t) = \sum_{k=0}^{N_t-1} y_1(t) + y_2(t) + z(t), \quad (1)$$

where $z(t)$ is a complex additive white Gaussian noise (AWGN) vector with zero mean and variance of σ^2 , $y_1(t)$ and $y_2(t)$ denote the echo signals from SBS₁ and SBS₂, respectively. The notation is defined as follows:

- k is the index of antenna elements.

The active sensing echo signal from SBS₁ and the passive sensing echo signal from SBS₂ can be expressed as [41]–[46]

$$y_1(t) = \sum_{m=0}^{M-1} \sum_{n=0}^{N-1} \overbrace{d_{1,\text{Tx}}(k, m, n) \times \sum_{l=0}^{L-1} \alpha_{1,l} e^{j\Omega_l k} e^{-j2\pi n \Delta f \tau_{1,l}} \times e^{j2\pi m T f_{D,1,l}}}^{d_{1,\text{Rx}}(k, m, n)} \quad (2)$$

$$\cdot e^{-j2\pi(f_{c1} + n\Delta f)t} \cdot \text{rect}\left(\frac{t - mT - \tau_{1,l}}{T}\right), \quad (3)$$

$$y_2(t) = \sum_{m=0}^{M-1} \sum_{n=0}^{N-1} \overbrace{d_{2,\text{Tx}}(k, m, n) \times \sum_{l=0}^{L-1} \alpha_{2,l} e^{j\Omega_l k} e^{-j2\pi n \Delta f (\tau_{2,l} + \delta_\tau(m))} \times e^{j2\pi m T (f_{D,2,l} + \delta_f(m))}}^{d_{2,\text{Rx}}(k, m, n)} \quad (4)$$

$$\cdot e^{-j2\pi(f_{c2} + n\Delta f)t} \cdot \text{rect}\left(\frac{t - mT - \tau_{2,l} - \delta_\tau(m)}{T}\right), \quad (5)$$

where $\text{rect}\{\cdot\}$ denotes a rectangular window function. The rest of the notations and terms can be defined as follows:

- $\mathbf{a}(\Omega_l)$ is the receive steering vector of the l -th target with $\Omega_l = \frac{2\pi d}{\lambda} \cos(\theta_l)$,
- d is the distance between adjacent antenna elements,
- λ is the wavelength of the signal,
- θ_l is the direction of the l -th target,
- M and N represent the number of OFDM symbols and the number of subcarriers,
- m and n are the indices of the OFDM symbols and the subcarriers, respectively,
- f_{c1} and f_{c2} are the carrier frequency of the active sensing and passive sensing echo signal,
- L is the number of targets,
- T is the length of an OFDM symbol,
- Δf is the carrier spacing of OFDM signals.

- $d_{1,\text{Rx}}(k, m, n)$ and $d_{2,\text{Rx}}(k, m, n)$ are the received modulation symbols of the k -th antenna on SBS₁ and SBS₂,
- $d_{1,\text{Tx}}(k, m, n)$ and $d_{2,\text{Tx}}(k, m, n)$ are the transmitted modulation symbols of the k -th antenna on SBS₁ and SBS₂,
- $\tau_{1,l}$ and $f_{D,1,l}$ are the delay and Doppler spread between the l -th target and SBS₁,
- $\tau_{2,l}$ and $f_{D,2,l}$ are the delay and Doppler spread between the l -th target and SBS₂,
- $\alpha_{1,l}$ and $\alpha_{2,l}$ are the channel fading magnitudes of the l -th target in active and passive sensing,
- $\delta_\tau(m)$ and $\delta_f(m)$ denote the unknown time-varying TO and CFO [23], [47].

III. DELAY AND DOPPLER SPREAD ESTIMATION BASED ON CCCS

According to Section II-B, the delay and Doppler spread are mixed with TOs and CFOs, respectively. In this section, we propose the CCCS based algorithm to mitigate TOs and CFOs for achieving high-accuracy target delay and Doppler spread estimation. The CCCS based algorithm for delay and Doppler spread estimation consists of the following steps.

A. Extracting Sensing Information

Based on (1), (4) and (5), the transmitted and received modulation symbols of the k -th antenna array from SBS₁ and SBS₂ can be rewritten as matrices, $\mathbf{D}_{1,\text{Tx}}(k)$, $\mathbf{D}_{2,\text{Tx}}(k)$, $\mathbf{D}_{1,\text{Rx}}(k)$, $\mathbf{D}_{2,\text{Rx}}(k)$, in which each column represents a OFDM symbol and each row represents a subcarrier. The sensing information can be extracted from the received modulation symbols by a point-wise complex division. Since the transmitted signal is modulated by quadrature phase shift keying (QPSK) in this paper, the amplitude of the transmitted OFDM modulation symbol is a non-zero constant, the noise enhancement caused by point-wise complex division is not serious [30]. Without loss of generality, we take the example of extracting sensing information from $\mathbf{D}_{1,\text{Rx}}(k)$ [48], [49]

$$\mathbf{D}_{\text{div}}(k) = \frac{\mathbf{D}_{1,\text{Rx}}(k)}{\mathbf{D}_{1,\text{Tx}}(k)} = \mathbf{k}_{1,R}(k) \otimes \mathbf{k}_{1,D}(k) \quad , \quad (6)$$

where \otimes is the Kronecker product operator and

$$\mathbf{k}_{1,R}(k) = \sum_{l=0}^{L-1} \alpha_{1,l} e^{j\Omega_l k} \left[1, \dots, e^{-j2\pi n \Delta f \tau_{1,l}}, \dots, e^{-j2\pi(N-1)\Delta f \tau_{1,l}} \right]^T \quad , \quad (7)$$

$$\mathbf{k}_{1,D}(k) = \sum_{l=0}^{L-1} \alpha_{1,l} e^{j\Omega_l k} \left[1, \dots, e^{j2\pi m T f_{D,1,l}}, \dots, e^{j2\pi(M-1)T f_{D,1,l}} \right]^T \quad , \quad (8)$$

are the range and Doppler spread steer vectors of active sensing.

Similarly, $\mathbf{k}_{2,R}(k)$ and $\mathbf{k}_{2,D}(k)$ can be obtained by extracting sensing information from from $\mathbf{D}_{2,Rx}$

$$\mathbf{k}_{2,R}(k) = \sum_{l=0}^{L-1} \alpha_{2,l} e^{j\Omega_l k} \left[1, \dots, e^{-j2\pi n \Delta f (\tau_{2,l} + \delta_\tau(m))}, \dots, e^{-j2\pi(N-1) \Delta f (\tau_{2,l} + \delta_\tau(m))} \right]^T, \quad (9)$$

$$\mathbf{k}_{2,D}(k) = \sum_{l=0}^{L-1} \alpha_{2,l} e^{j\Omega_l k} \left[1, \dots, e^{j2\pi m T (f_{D,2,l} + \delta_f(m))}, \dots, e^{j2\pi(M-1) T (f_{D,2,l} + \delta_f(m))} \right]^T. \quad (10)$$

B. Deviation Analysis of Cooperative Active and Passive Sensing

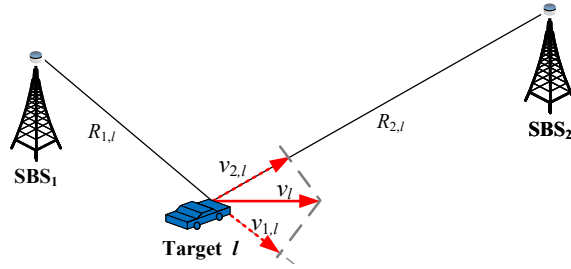


Fig. 2: Active and passive sensing for the l -th target.

Due to the different location information of SBS₁ and SBS₂, there are deviations in the delay and Doppler spread estimation of active and passive sensing for the same target, which needs to be mitigated in order to achieve high accurate cooperative sensing. Without loss of generality, we consider the active and passive sensing for the l -th target. As Fig. 2 shows, the distance from the l -th target to SBS₁ and SBS₂ is $R_{1,l}$ and $R_{2,l}$, the velocity of target in the direction of SBS₁ and SBS₂ is $v_{1,l}$ and $v_{2,l}$. The delay, $\tau_{1,l}$ and $\tau_{2,l}$ can be expressed as

$$\tau_{1,l} = \frac{2R_{1,l}}{c}, \quad \tau_{2,l} = \frac{R_{1,l} + R_{2,l}}{c}, \quad (11)$$

where c is the speed of signal, $R_{1,l}$ and $R_{2,l}$ are the range from the l -th target to SBS₁ and SBS₂, respectively. Then the deviation of active and passive sensing in terms of delay estimation is

$$\Delta\tau_l = \tau_{2,l} - \tau_{1,l} = \frac{R_{2,l} - R_{1,l}}{c}. \quad (12)$$

Similarly, the Doppler spread, $f_{D,1,l}$ and $f_{D,2,l}$ can be expressed as

$$f_{D,1,l} = \frac{2v_{1,l}f_{c1}}{c}, \quad f_{D,2,l} = \frac{(v_{1,l} - v_{2,l})f_{c2}}{c}, \quad (13)$$

and the deviation of active and passive sensing in terms of Doppler spread estimation $\Delta f_{D,l}$ can be derived as

$$\Delta f_{D,l} = f_{D,2,l} - f_{D,1,l} = \frac{v_{1,l}(f_{c2} - f_{c1})}{c} - \frac{(v_{1,l} + v_{2,l})f_{c2}}{c}, \quad (14)$$

where $v_{1,l}$ and $v_{2,l}$ are the velocity of the l -th target in the direction from SBS₁ to the l -th target and from the l -th target to SBS₂.

C. CCCS for Mitigating TOs and CFOs

To obtain better sensing performance by fusing the sensing signals of active and passive sensing, it is necessary to mitigate TOs and delay deviation of passive sensing in range measurement, and to mitigate the CFOs and Doppler spread deviation of passive sensing in velocity measurement. The CCCS based algorithm is proposed to mitigate TOs plus delay deviation and CFOs plus Doppler spread deviation by correlating active and passive sensing information. Specifically, the CCCS based algorithm regards the active sensing echo signal as a reference signal, and mitigates TOs and CFOs in the passive sensing echo signal by correlating the active and passive echo signals, which is named the CCCS algorithm.

1) *Single target*: For single target, i.e., $L = 1$, we perform the same CCCS algorithm for the received signal on each antenna. Without loss of generality, taking the 0-th antenna as an example, i.e., $k = 0$, then $e^{j\Omega_l k} = 1$. Then, the active and passive sensing information normalized vectors can be re-expressed as

$$\begin{aligned} \mathbf{k}_{1,R} &= \left[1, \dots, e^{-j2\pi(N-1)\Delta f\tau_1} \right]^T, & \mathbf{k}_{1,D} &= \left[1, \dots, e^{j2\pi(M-1)Tf_{D,1}} \right]^T, \\ \mathbf{k}_{2,R} &= \left[1, \dots, e^{-j2\pi(N-1)\Delta f(\tau_2 + \delta_\tau(m))} \right]^T, & \mathbf{k}_{2,D} &= \left[1, \dots, e^{j2\pi(M-1)T(f_{D,2} + \delta_f(m))} \right]^T. \end{aligned} \quad (15)$$

Deviations of delay and Doppler spread between active and passive sensing for the same target can be re-expressed as $\Delta\tau$ and Δf_D , respectively. For mitigating $\Delta\tau + \delta_\tau(m)$, the CCCS algorithm between $\mathbf{k}_{1,R}$ and $\mathbf{k}_{2,R}$ generates

$$\rho_R = \text{diag}(\mathbf{k}_{2,R}^H) \cdot \mathbf{k}_{1,R} = \left[1, \dots, e^{j2\pi n\Delta f(\Delta\tau + \delta_\tau(m))}, \dots, e^{j2\pi(N-1)\Delta f(\Delta\tau + \delta_\tau(m))} \right]^T. \quad (16)$$

For mitigating $\Delta f_D + \delta_f(m)$, the CCCS algorithm between $\mathbf{k}_{1,D}$ and $\mathbf{k}_{2,D}$ generates

$$\rho_D = \text{diag}(\mathbf{k}_{2,D}^H) \cdot \mathbf{k}_{1,D} = \left[1, \dots, e^{-j2\pi mT(\Delta f_D + \delta_f(m))}, \dots, e^{-j2\pi(M-1)T(\Delta f_D + \delta_f(m))} \right]^T. \quad (17)$$

where $\Delta\tau + \delta_\tau(m)$ translates into a linear phase shift between the modulation symbols along the carrier frequency axis, $\Delta f_D + \delta_f(m)$ translates into a linear phase shift between the modulation symbols along the OFDM symbol axis. Thus, $\Delta\tau + \delta_\tau(m)$ and $\Delta f_D + \delta_f(m)$ can be estimated by the discrete Fourier transform (DFT) algorithm [48].

2) *Multiple targets*: Compared with the single target scenario, it is more difficult to obtain TOs and CFOs for multiple targets by CCCS algorithm because of the problem of inter-target correlation interference. To overcome this challenge, we propose a multi-target alignment algorithm to handle the outputs of the CCCS method for multiple targets.

According to (7), (8), (9) and (10), we can obtain the active sensing information vector, $\mathbf{k}_{1,R}(k)$, $\mathbf{k}_{2,R}(k)$ and passive sensing information vector, $\mathbf{k}_{1,D}(k)$, $\mathbf{k}_{2,D}(k)$. For mitigating $\Delta\tau_l + \delta_\tau(m)$, the CCCS algorithm between $\mathbf{k}_{1,R}(k)$ and $\mathbf{k}_{2,R}(k)$ generates

$$\rho_R(k) = \text{diag}(\mathbf{k}_{2,R}^H(k)) \cdot \mathbf{k}_{1,R}(k) = \left[\beta_R(0, k), \dots, \beta_R(n, k), \dots, \beta_R(N-1, k) \right]^T, \quad (18)$$

where

$$\beta_R(n, k) = \sum_{l_1=0}^{L-1} \sum_{l_2=0}^{L-1} \alpha_{1,l_1} \alpha_{2,l_2} \cdot e^{j(\Omega_{l_1} - \Omega_{l_2})k} e^{j2\pi n \Delta f (\tau_{2,l_2} - \tau_{1,l_1} + \delta_\tau(m))}, \quad (19)$$

which can be split into two parts, $D_R(n, k)$ and $I_R(n, k)$.

$$\begin{aligned} D_R(n, k) &= \sum_{l=0}^{L-1} \alpha_{1,l} \alpha_{2,l} e^{j(\Omega_l - \Omega_l)k} e^{j2\pi n \Delta f (\tau_{2,l} - \tau_{1,l} + \delta_\tau(m))} \\ &= \sum_{l=0}^{L-1} \alpha_{1,l} \alpha_{2,l} e^{j2\pi n \Delta f (\Delta\tau_l + \delta_\tau(m))} \end{aligned}, \quad (20)$$

$$I_R(n, k) = \sum_{l_1=0}^{L-1} \sum_{l_2=0, l_2 \neq l_1}^{L-1} \alpha_{1,l_1} \alpha_{2,l_2} e^{j(\Omega_{l_1} - \Omega_{l_2})k} \cdot e^{j2\pi n \Delta f (\tau_{2,l_2} - \tau_{1,l_1} + \delta_\tau(m))}. \quad (21)$$

According to (19), (20) and (21), the CCCS outputs for multiple targets not only contains information on TOs and CFOs of the same target, $D_R(n, k)$, but also time delay and Doppler spread correlation information between different targets, $I_R(n, k)$, which will interfere with the subsequent TOs and CFOs mitigation operations. To overcome this problem, we propose a CCCS based algorithm for multiple targets, including two stages, i.e., the extraction stage and the matching stage. In the extraction stage, we conduct $\delta_\tau(m) + \Delta\tau_l$ and $\Delta\tau + \Delta f_{D,l}$ extraction without differentiating between different targets, and we match them for different targets in the matching stage.

For above CCCS outputs, we have the proposition that $D_R(n, k)$ is invariant with k and $I_R(n, k)$ is variant with k . Based on the above proposition, we can firstly obtain the set of phase information in $\beta_R(n, k)$ by the DFT algorithm [48]. Then, the phase set of $D_R(n, k)$ can be extracted by continuously adjusting k , observing whether the DFT output of corresponding phases change, as shown in Algorithm 1.

Algorithm 1 $\Delta\tau_l + \delta_\tau(m)$ extraction method

Input:

- The CCCS output based on (18), $\rho_R(k)$,
- the n -th element of $\rho_R(k)$ based on (19), $\beta_R(n, k)$,
- the index of antenna, $k = 0$,
- the threshold, ε_1 .

Step 1: Calculate the vector sum of $\beta_R(n, k)$ on the N_t antennas to enhance $D_R(n, k)$.

$$D_R(n) = \sum_{k=0}^{\rightarrow N_t-1} D_R(n, k) = N_t \sum_{l=0}^{L-1} \alpha_{1,l} \alpha_{2,l} e^{j2\pi n \Delta f (\Delta\tau_l + \delta_\tau(m))}, \quad (22)$$

$$I_R(n) = \sum_{k=0}^{\rightarrow N_t} I_R(n, k) = \sum_{l_1=0}^{L-1} \sum_{l_2=0, l_2 \neq l_1}^{L-1} \sum_{k=0}^{\rightarrow N_t-1} e^{j(\Omega_{l_2} - \Omega_{l_1})k} \alpha_{1,l_1} \alpha_{2,l_2} e^{j2\pi n \Delta f (\tau_{2,l_2} - \tau_{1,l_1} + \delta_\tau(m))}. \quad (23)$$

Proof: The proof is provided in Appendix A.

Step 2:

2a) Perform the DFT operation on $\rho_R(k)$

$$r(q_k) = \text{DFT}(\rho_R(k)) = \sum_{n=0}^{N-1} \rho_R(k) e^{-j \frac{2\pi}{N} n q_k \Delta f}. \quad (24)$$

2b) Generate P_k , which is the set of the delay information, $q_{k,i}$, and the real part of the DFT output, $\text{real}(r(q_{k,i}))$.

$$P_k = \mathcal{S}(q_{k,i}, \text{real}(r(q_{k,i}))), i = 0, 1, \dots, L^2, \quad (25)$$

$$q_{k,i} = \lfloor N \Delta f (\tau_{2,l_2} - \tau_{1,l_1} + \delta_\tau(m)) \rfloor, \quad (26)$$

where $\mathcal{S}(x_i)$ denotes the set of x_i , $q_{k,i}$ denotes the index of peak of DFT outputs, $r(q_{k,i})$ denotes the value of peak of DFT outputs.

Step 3: Extract $\Delta\tau_l + \delta_\tau(m)$ by adjust k , where $\Delta\tau_l = \tau_{2,l} - \tau_{1,l}$.

3a) Generate $P_0 = \mathcal{S}(q_{0,i}, \text{real}(r(q_{0,i})))$ based on step 2.

while $k \leq N_t$ and P_0 is updated **do**

$k = k + 1$.

3b) Generate P_k based on step 2.

for all $(q_{0,i}, \text{real}(r(q_{0,i})))$ in P_0 **do**

if $|\text{real}(r(q_{0,i})) - \text{real}(r(q_{k,i}))| \geq \varepsilon_1$ **then**

3c) Remove $(q_{0,i}, \text{real}(r(q_{0,i})))$ from P_0 .

end if

end for

end while

Output: P_0 .

So far, $\Delta\tau_l + \delta_\tau(m)$ has been estimated, which can be expressed as

$$P_g = \mathcal{S}(\Delta\tau_0 + \delta_\tau(m), \dots, \Delta\tau_l + \delta_\tau(m), \dots, \Delta\tau_{L-1} + \delta_\tau(m)) \quad (27)$$

The delay estimation of active and passive sensing can be obtained by DFT [48]

$$\begin{aligned} P_m &= \mathcal{S}(\tau_{1,0}, \dots, \tau_{1,l}, \dots, \tau_{1,L-1}) \\ P_b &= \mathcal{S}(\tau_{2,0} + \delta_\tau(m), \dots, \tau_{2,l} + \delta_\tau(m), \dots, \tau_{2,L-1} + \delta_\tau(m)) \end{aligned} \quad (28)$$

Although $\Delta\tau_l + \delta_\tau(m)$ has been estimated in P_g , there is a mismatch between P_g and P_m and P_b . Recognizing this fact, we propose a matching method to achieve the matching of active and passive delay estimation of different targets, as shown in Algorithm 2.

Algorithm 2 Matching method for delay estimation of different targets

Input:

- P_b, P_m, P_g ,
 - the threshold, ε_2 ,
 - the empty matching set, $C_R = \mathcal{S}(\cdot)$.
- for** $P_g(i)$ in P_g and $P_m(i)$ in P_m and $P_b(i)$ in P_b **do**
- if** $|P_m(i) + P_g(i) - P_b(i)| \leq \varepsilon_2$ **then**
- Add $(P_m(i), P_g(i), P_b(i))$ to C_R .
- end if**
- end for**

Output: C_R .

As for mitigating $\Delta f_{D,l} + \delta_f(m)$, the outputs of the CCCS algorithm between $\mathbf{k}_{1,D}(k)$ and $\mathbf{k}_{2,D}(k)$ can be expressed as

$$\begin{aligned} \rho_V(k) &= \text{diag}(\mathbf{k}_{2,D}^H(k)) \cdot \mathbf{k}_{1,D}(k) \\ &= \left[\beta_V(0, k), \dots, \beta_V(m, k), \dots, \beta_V(M-1, k) \right]^T, \end{aligned} \quad (29)$$

where

$$\beta_V(m, k) = \sum_{l_1=0}^{L-1} \sum_{l_2=0}^{L-1} \alpha_{1,l_1} \alpha_{2,l_2} e^{j(\Omega_{l_1} - \Omega_{l_2})k} \cdot e^{j2\pi m T (f_{D,2,l_2} - f_{D,1,l_1} + \delta_f(m))}, \quad (30)$$

which can be split into two parts, $D_V(m, k)$ and $I_V(m, k)$.

$$\begin{aligned} D_V(m, k) &= \sum_{l_1=0}^{L-1} \sum_{l_2=0, l_2=l_1}^{L-1} \alpha_{1,l_1} \alpha_{2,l_2} e^{j(\Omega_{l_1} - \Omega_{l_2})k} \cdot e^{j2\pi m T (f_{D,2,l_2} - f_{D,1,l_1} + \delta_f(m))} \\ &= \sum_{l=0}^{L-1} \alpha_{1,l} \alpha_{2,l} e^{j(\Omega_l - \Omega_l)k} e^{j2\pi m T (\Delta f_{D,l} + \delta_f(m))}, \end{aligned} \quad (31)$$

$$\begin{aligned} I_V(m, k) &= \sum_{l_1=0}^{L-1} \sum_{l_2=0, l_2 \neq l_1}^{L-1} \alpha_{1,l_1} \alpha_{2,l_2} e^{j(\Omega_{l_1} - \Omega_{l_2})k} \cdot e^{j2\pi m T (f_{D,2,l_2} - f_{D,1,l_1} + \delta_f(m))}. \end{aligned} \quad (32)$$

Similarly, $D_V(m)$ can be obtained by an operation like (22). Most operation of CCCS for mitigating $\Delta f_{D,l} + \delta_f(m)$ is similar to that for mitigating $\Delta f_{D,l} + \delta_f(m)$, which has been introduced above. The main difference is how to extract the Doppler information from $D_V(m)$.

For case 1: CFO is almost constant within the sensing signal containing M OFDM symbols,

$$\delta_f(0) \approx, \dots, \approx \delta_f(m) \approx, \dots, \approx \delta_f(M-1). \quad (33)$$

Then, $\Delta f_{D,l} + \delta_f(m)$ is invariant with m , which means that the Doppler information from $D_V(m)$ can be obtained by DFT.

For case 2: CFO is not a constant within the sensing signal containing M OFDM symbols,

$$\delta_f(0) \neq, \dots, \neq \delta_f(m) =, \dots, \neq \delta_f(M-1). \quad (34)$$

Then, $\Delta f_{D,l} + \delta_f(m)$ is variant with m , which means that the Doppler information from $D_V(m)$ cannot be obtained by the DFT algorithm. Therefore, the performance of CCCS for mitigating $\Delta f_{D,l} + \delta_f(m)$ is affected by the variance of CFO, which will be analyzed and simulated in detail in Section V.

D. Delay and Doppler spread Estimation by two dimensional (2D) DFT

As mentioned in Section III-C, after mitigating $\Delta\tau_l + \delta\tau(m)$ and $\Delta f_{D,l} + \delta f(m)$, the active and passive sensing information vector can be translated into a linear phase shift in the modulation symbols and the carrier frequency domain. The most convenient way to evaluate the range to the targets, is to compute inverse DFT (IDFT) of the range steer vector

$$r(i) = \frac{1}{N_I} \sum_{n=0}^{N_I-1} \sum_{l=0}^{L-1} (\alpha_{1,l} + \alpha_{2,l}) e^{-j2\pi n \Delta f(\tau_{1,l})} e^{j \frac{2\pi}{N_I} ni}, \quad i = 0, 1, \dots, N_I - 1, \quad (35)$$

where N_I is the number of IDFT points. It can be seen that, the two exponential terms in (35) cancel each other and result in unity, under the condition

$$i = \lfloor \Delta f N_I \tau_{1,l} \rfloor, \quad (36)$$

where $\lfloor \cdot \rfloor$ denotes the operation of round down. It means that a peak will occur at this index of i in the time response $r(i)$. Similarly, the estimation of Doppler spread can be solved by applying DFT to the Doppler spread steer vector

$$v(i) = \sum_{m=0}^{M_D-1} \sum_{l=0}^{L-1} (\alpha_{1,l} + \alpha_{2,l}) e^{j2\pi m T f_{D,1,l}} e^{-j \frac{2\pi}{M_D} mi}, \quad i = 0, 1, \dots, M_D - 1, \quad (37)$$

where M_D is the number of DFT points. Cancellation of the exponential terms, and constructive superposition, results for the index

$$i = \lfloor T M_D f_{D,1,l} \rfloor. \quad (38)$$

Then, delay and Doppler spread of the l -th target can be estimated based on (37) and (38). Further, ranging and velocity measurement can be realized by (11) and (13).

E. Complexity Analysis

TABLE I: Complexity of Delay and Doppler spread estimation

Operation	CCCS	Algorithm 1	Algorithm 2	2D DFT	Overall
Delay estimation	$\mathcal{O}(N^2 \times N_t)$	$N \log(N) \times N_t$	$\mathcal{O}(L^3)$	$\mathcal{O}(N \log(N))$	$\mathcal{O}(N^2 \times N_t + L^3)$
Doppler spread estimation	$\mathcal{O}(M^2 \times M_t)$	$M \log(M) \times N_t$	$\mathcal{O}(L^3)$	$\mathcal{O}(M \log(M))$	$\mathcal{O}(M^2 \times N_t + L^3)$

In this subsection, we analyze the computational complexity of cooperative sensing for delay and Doppler spread estimation. Since the delay and Doppler spread are estimated in parallel,

without loss of generality, we only analyze the complexity of the delay estimation. There are four main computations, CCCS, Algorithm 1, Algorithm 2 and delay estimation by DFT. Since the size of $\mathbf{k}_{1,R}(k)$ is $1 \times N$ and the size of $\text{diag}(\mathbf{k}_{2,R}(k))$ is $N \times N$, the complexities of CCCS is $\mathcal{O}(N^2)$. For N_t antennas, the complexities of CCCS is $\mathcal{O}(N^2 \times N_t)$. In Algorithm 1, the complexity of calculating the vector sum of $\beta_R(n, k)$ with the dimension of 1×1 on N_t antennas is $\mathcal{O}(N_t)$, the complexity of step 2 is $\mathcal{O}(N \log(N))$, for N_t antennas, the complexity is updated to $N \log(N) \times N_t$. In Algorithm 2, since the size of P_m , P_b and P_g are all close to $1 \times L$, the complexities of matching method is $\mathcal{O}(L^3)$. According to [48], the complexities of DFT is $\mathcal{O}(N \log(N))$. Therefore, the overall complexity for estimating delay is $\mathcal{O}(N^2 \times N_t + L^3)$. Likewise, the overall complexity for estimating Doppler spread can be derived as $\mathcal{O}(M^2 \times N_t + L^3)$. The details of complexity analysis are summarized in Table I

IV. AO A ESTIMATION BASED ON COOPERATIVE SENSING

In this section, we propose a low complexity AoA estimation algorithm based on cooperative sensing, which contains two stages, i.e., the coarse AoA estimation (CAE) stage and the fine AoA estimation (FAE) stage. In the CAE stage, we obtain a rough AoA estimation of targets by cooperative active and passive sensing. In the FAE stage, we can obtain a fine AoA of targets by FRFT algorithm within the range of rough AoA estimation.

A. CAE by Cooperative Sensing

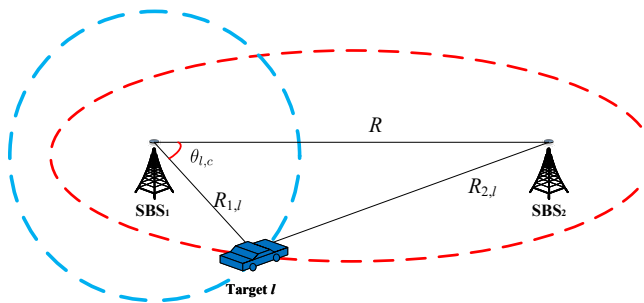


Fig. 3: CAE by cooperative sensing.

As Fig. 3 shows, the distance between SBS_1 and SBS_2 is R , the ranging result of active sensing is $R_{1,l}$, the ranging result of passive sensing is $R_{1,l} + R_{2,l}$. Then the rough AoA estimated result

of the l -th target, $\Omega_{l,c}$ can be expressed as

$$\begin{aligned}\theta_{l,c} &= \arccos\left(\frac{R_{1,l}^2 + R^2 - R_{2,l}^2}{2RR_{1,l}}\right) \\ \Omega_{l,c} &= \frac{2\pi d}{\lambda} \cos(\theta_{l,c}) = \frac{2\pi d}{\lambda} \cdot \frac{R_{1,l}^2 + R^2 - R_{2,l}^2}{2RR_{1,l}},\end{aligned}\quad (39)$$

B. FAE by FRFT

The accuracy of $\Omega_{l,c}$ is not high because there are errors in the ranging results of active and passive sensing. To obtain high accuracy AoA estimation, we adopt the FRFT algorithm [29] for the received steer vector of targets

$$\text{AoA}(i) = \sum_{k=0}^{N_t N_f - 1} \sum_{l=0}^{L-1} e^{j\Omega_l k} e^{-j \frac{2\pi}{N_t N_f} k i}, \quad i = 0, 1, \dots, N_t N_f, \quad (40)$$

where N_f is the fractional index of FRFT. However, the complexity of FRFT is $\mathcal{O}(N_t^2 N_f^2)$, which gets larger squared as N_f gets larger. To decrease the complexity of FRFT, we adopt the FRFT algorithm within the range of $[\Omega_{l,c} - \Omega, \Omega_{l,c} + \Omega]$

$$\text{AoA}(i) = \sum_{k=0}^{N_t N_f - 1} \sum_{l=0}^{L-1} e^{j\Omega_l k} e^{-j \frac{2\pi}{N_t N_f} k i}, \quad i = i_s, \dots, i_e, \quad (41)$$

$$\begin{aligned}i_s &= \left\lfloor \frac{N_t N_f (\Omega_{l,c} - \Omega)}{2\pi} \right\rfloor \\ i_e &= \left\lceil \frac{N_t N_f (\Omega_{l,c} + \Omega)}{2\pi} \right\rceil,\end{aligned}\quad (42)$$

where Ω is the uncertainty range of $\Omega_{l,c}$. Then, the fine AoA estimated result, $\Omega_{l,f}$ can be derived as

$$\begin{aligned}\Omega_{l,f} &\in \left[\frac{2\pi i_l}{N_t N_f}, \frac{2\pi i_l}{N_t N_f} + 1 \right) \\ \theta_{l,f} &\in \left[\arccos\left(\frac{\lambda i_l}{d N_t N_f}\right), \arccos\left(\frac{\lambda i_l}{d N_t N_f} + \frac{\lambda}{2\pi d}\right) \right),\end{aligned}\quad (43)$$

where i_l is the index of the peak of $\text{AoA}(i)$.

Algorithm 3 AoA estimation based on cooperative sensing

Input: The waveform length λ , the distance between two adjacent antenna elements d , the received steer vector $\mathbf{a}(\Omega_1)$, the ranging results of active and passive sensing $R_{1,l}$, $R_{1,l} + R_{2,l}$, the uncertainty range, Ω ;

1) CAE by cooperative sensing:

1a) Obtain coarse AoA estimated result, $\Omega_{l,c}$ according to (39).

2) FAE by FRFT:

2a) Determine the range of FRFT based on (42).

2b) Obtain the fine AoA estimated result, $\Omega_{l,c}$ according to (41) and (43).

Output: $\Omega_{l,f}$.

C. Complexity Analysis

In this subsection, we analyze the computational complexity of Algorithm 3, which includes two parts. In the CAE stage, the complexity of obtaining $\Omega_{l,c}$ is $\mathcal{O}(1)$. In the FAE stage, the complexity of FRFT based on the rough AoA estimation is $\mathcal{O}\left(\frac{N_t^2 N_f^2 \Omega}{\pi}\right)$. Therefore, the overall computational complexity of Algorithm 3 is $\mathcal{O}\left(\frac{N_t^2 N_f^2 \Omega}{\pi}\right)$, which is $\frac{\Omega}{\pi}$ times less complex than the traditional FRFT algorithm. The complexities of the main steps of AoA estimation are summarized in Table II and are compared with those of the traditional FRFT method.

TABLE II: Complexity of AoA estimation

Operation	CAE based on cooperative sensing	FRFT with CAE	FRFT without CAE	Overall
Algorithm 3	$\mathcal{O}(1)$	$\mathcal{O}\left(\frac{N_t^2 N_f^2 \Omega}{\pi}\right)$		$\mathcal{O}\left(\frac{N_t^2 N_f^2 \Omega}{\pi}\right)$
Traditional FRFT			$\mathcal{O}(N_t^2 N_f^2)$	$\mathcal{O}(N_t^2 N_f^2)$

V. SIMULATION RESULTS

In this section, we first analyze and simulate the accuracy of range and velocity estimation of passive sensing with TOs and CFOs, and then analyze the performance improvement in delay, Doppler spread and AoA estimation. Simulation parameters used in this section are shown in table III [12], [47], [50].

A. Range and Velocity Estimation of Passive Sensing with TOs and CFOs

In this section, we analyze and simulate the performance of passive sensing with TOs and CFOs. Fig. 4 presents the normalized mean-squared-error (NMSE) for range and velocity, which can be expressed as

$$\Gamma_R = \frac{1}{L} \sum_{l=0}^{L-1} \frac{|R_{e,l} - R_{r,l}|^2}{R_{r,l}^2}, \quad \Gamma_V = \frac{1}{L} \sum_{l=0}^{L-1} \frac{|V_{e,l} - V_{r,l}|^2}{V_{r,l}^2}, \quad (44)$$

TABLE III: Simulation parameters adopted in this paper.

Items	Value	Meaning of the parameter	Items	Value	Meaning of the parameter
f_{c1}	4 GHz [50]	Carrier frequency of active sensing	f_{c2}	4.2 GHz [50]	Carrier frequency of passive sensing
c	$3 \cdot 10^8$ m/s	Speed of light	Δf	120 kHz [50]	Carrier frequency
M	256 [12]	Number of OFDM symbols	N	1024 [50]	Number of subcarriers
M_D	2560	Number of DFT points	N_I	10240	Number of IDFT points
T	10.38 us [50]	The whole OFDM period	B	123 MHz [50]	Frequency bandwidth
N_t	[4,8] [12]	Number of antenna array	L	[3,5]	Number of targets
R_l	[70,100,130]m	Range of targets	V_l	[15,25,35]m/s	Velocity of targets
θ_l	[25, 30, 35] $^\circ$	AoA of targets	SNR_m	[-30,30] dB	SNR of active sensing received signals
SNR_b	[-30,30] dB	SNR of passive sensing received signals	SNR_r	$\frac{\text{SNR}_b}{\text{SNR}_m}$	Power ratio between two types of sensing
$E(\delta_\tau)$	[10,1000] ns	Mean of TOs	$E(\delta_f)$	[0.01,0.2] Δf	Mean of CFOs
$V(\delta_\tau)$	[1,100] ns	Variance of TOs	$V(\delta_f)$	[0.01,0.2] Δf	Variance of CFOs
ε_1	0.01	Threshold in Algorithm 1	ε_2	0.01	Threshold in Algorithm 2

where $R_{r,l}$ and $V_{r,l}$ are the actual range and velocity of targets, $R_{e,l}$ and $V_{e,l}$ are the estimated range and velocity. As Fig. 4(a) and Fig. 4(b) show that the effect of TOs on velocity estimation is greater than that no range estimation, which is consistent with the theoretical analysis. Under the condition of low SNR_b , NMSE of range Γ_R is large and the performance of range estimation is poor, and the larger the mean value of TOs $E(\delta_\tau)$ is, the larger the fluctuation of Γ_R is. As SNR_b is raised, Γ_R is stable. In the meanwhile, the larger $E(\delta_\tau)$ is, the larger Γ_R is, leading to poorer ranging performance. Moreover, by comparing the solid line and the dashed line in Fig. 4(a), it can be found that the solid line is close to the dashed line under the condition of the same $E(\delta_\tau)$, which means that the variance of TOs $V(\delta_\tau)$ does not have a great influence on the range estimation.

Fig. 4(c) and Fig. 4(d) present the NMSE of range and velocity with TOs and CFOs. According to Fig. 4(c), Γ_R decreases as SNR_b increases and gradually stabilizes, and CFOs have little effect on the stable Γ_R . However, when the mean value of CFOs $E(\delta_f)$ is $0.2\Delta f$, SNR_b required for Γ_R stabilization is larger due to the ICI caused by CFOs, which in turn affects the range estimation at low SNR_b conditions. According to the solid line in Fig. 4(d), under the condition of low variance of CFOs $V(\delta_f)$, NMSE of velocity Γ_V will gradually stabilizes with high SNR_b , but Γ_V increases with the increase of the mean value of CFOs $E(\delta_f)$. While the dashed line in in Fig. 4(d) fluctuates a lot in high areas, which means that the performance of velocity estimation

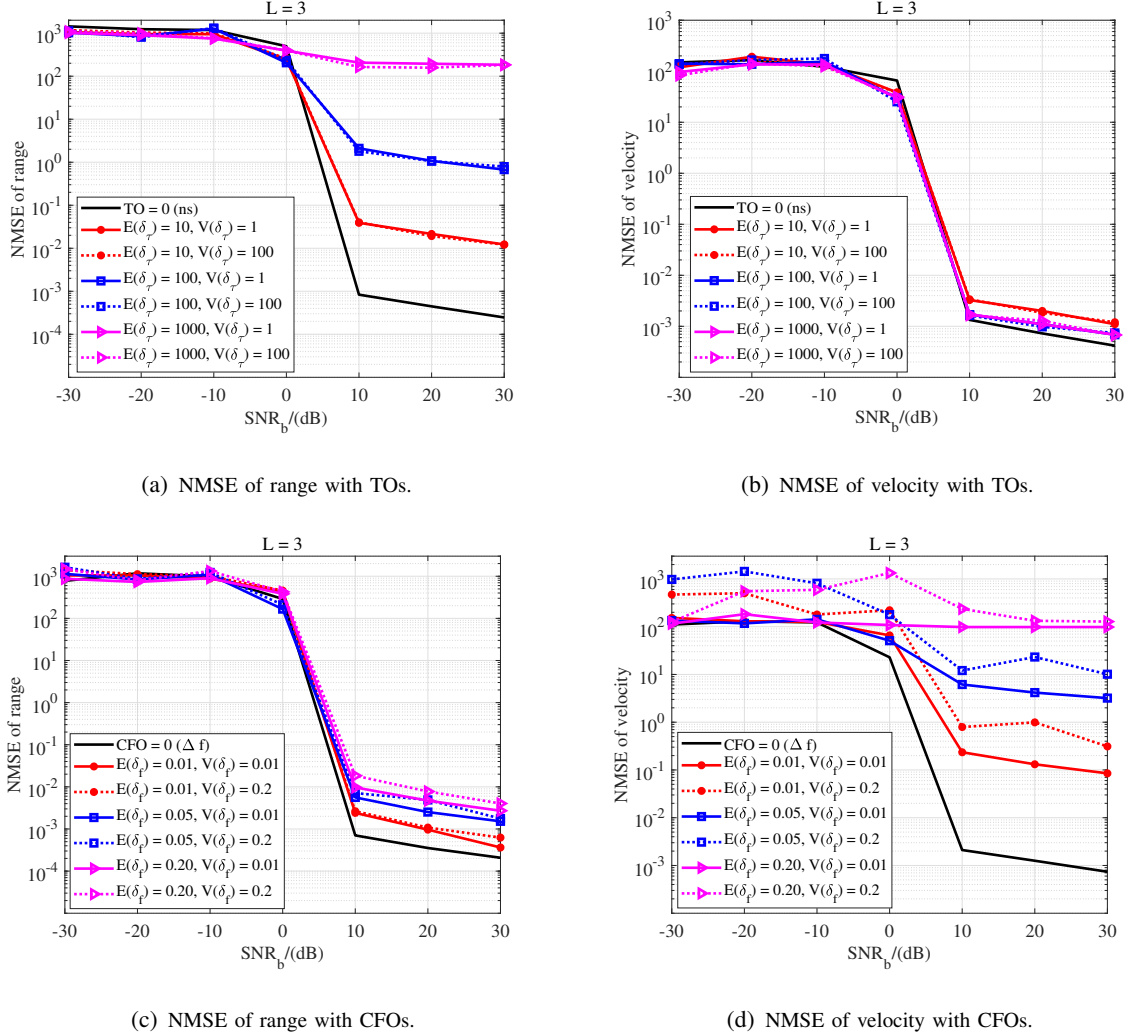


Fig. 4: NMSE of range and velocity with TOs and CFOs.

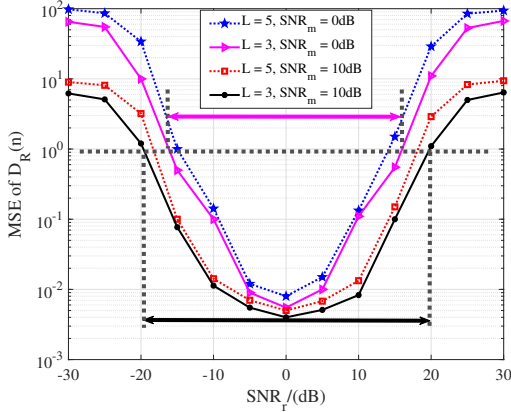
is poor when the variance of CFOs $V(\delta_f)$ is large.

B. Sensing Performance Enhancement by Cooperative Sensing

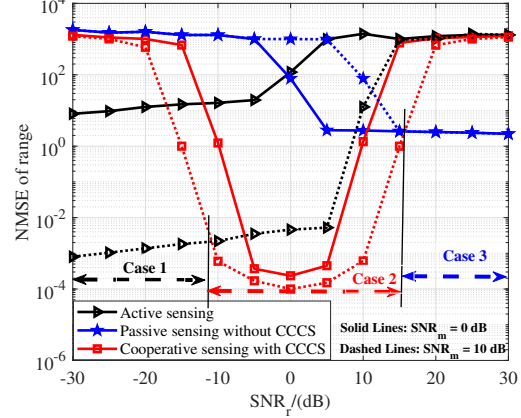
According to the analysis introduced in Section III-D, after CCCS, cooperative sensing can improve the sensing performance by fusing active and passive sensing signals, which can be manifested in two aspects: target estimation and detection.

1) *NMSE of range and velocity of cooperative sensing after CCCS*: The NMSE of range and velocity is an important metric for target estimation. In this section, we compared the performance enhancement effect of cooperative sensing on active and passive sensing for different power

ratios between them. Finally, the NMSE of range and velocity of passive sensing after CCCS is analyzed and simulated to verify the improvement of passive sensing performance by CCCS. MSE of $D_R(n)$ and $D_V(m)$ mentioned in Section III-C reflects the accuracy of the CCCS



(a) MSE of $D_R(n)$ versus power ratio SNR_r .



(b) NMSE of range with $\text{SNR}_m = 0\text{dB}$, $L = 3$.

Fig. 5: Sensing performance enhancement of cooperative sensing for different power ratios SNR_r with $E(\delta_f) = 0.2 \Delta f$, $E(\delta_\tau) = 100$ ns, $V(\delta_f) = 0.01$ and $V(\delta_\tau) = 100$.

outputs and directly impacts the sensing performance including NMSE of range Γ_R and NMSE of velocity Γ_V . According to Section III-C, $D_R(n)$ is obtained by correlating the active sensing and passive sensing, which means that the power ratio between the two types of sensing, defined as $\text{SNR}_r = \frac{\text{SNR}_b}{\text{SNR}_m}$, may affect the accuracy of $D_R(n)$. Fig. 5(a) presents MSE of $D_R(n)$ versus SNR_r with different SNR_m and number of targets. We can see that MSE of $D_R(n)$ decreases and then increases as SNR_r increases. MSE of $D_R(n)$ is relatively smaller when the absolute value of SNR_r is smaller, i.e., the power of active sensing is closer to that of passive sensing, which implies a higher estimation accuracy. By comparing the curves under different SNR_m in Fig. 5(a), it can be found that when the SNR_m is larger, the wider the range of SNR_r that satisfies the MSE of $D_R(n)$ less than a defined threshold, such as 1, which means that the larger the SNR_m , the CCCS can achieve TO and CFO estimation at a larger $|\text{SNR}_r|$, and the system is more robust.

We will further analyze the performance enhancement effect of the cooperation based joint active and passive sensing for different SNR_r . Without loss of generality, assuming that $\text{SNR}_m = 0$ dB, $L = 3$, $E(\delta_f) = 0.2 \Delta f$, $E(\delta_\tau) = 100$ ns, $V(\delta_f) = 0.01$ and $V(\delta_\tau) = 100$. We take

NMSE of range as an example to analyze the improvement of cooperative performance under different power ratios SNR_t . As Fig. 5(b) shows, we can see that:

- For active sensing, where the received signal of passive sensing is considered interference. When SNR_t is small, NMSE of range Γ_R is relatively low. With SNR_t increases, gradual enhancement of passive sensing received signals will interfere with active sensing received signals and causes Γ_R to be larger.
- For passive sensing, where the received signal of active sensing is considered interference. When SNR_t is small, Γ_R is relatively high. With SNR_t increases, gradual enhancement of passive sensing received signals makes Γ_R become smaller. However, Γ_R for passive sensing does not drop very low due to the impact of TOs and CFOs.
- For cooperation based joint active and passive sensing, where two sensing signals are fused by CCCS. When SNR_t is small, i.e., SNR_b is small, Γ_R for cooperative sensing is relatively high, close to that for passive sensing. With SNR_t increases, Γ_R for cooperative sensing is decreasing, lower than that for active sensing. But as SNR_t increases further, MSE of $D_R(n)$ increases as well, which has been analyzed above, leading to higher Γ_R for cooperative sensing.

Therefore, we can conclude that:

- when the received signal power of active sensing is much higher than that of passive sensing, i.e., case 1 as shown in Fig. 5(b), the sensing performance of active sensing is the best.
- when the received signal power of active sensing is close to that of passive sensing, i.e., case 2 as shown in Fig. 5(b), the sensing performance of cooperation based joint active and passive sensing is the best.
- when the received signal power of active sensing is much lower than that of passive sensing, i.e., case 3 as shown in Fig. 5(b), the sensing performance of passive sensing is the best.

To further analyze the improvement of cooperative sensing after CCCS in NMSE of range and velocity, we simulate the NMSE of range and velocity with different TOs, CFOs and number of targets. Without loss of generality, assuming that $\text{SNR}_t = 0$ dB, $E(\delta_f) = 0.2 \Delta f$, $E(\delta_\tau) = 100$ ns and $V(\delta_\tau) = 100$. Fig. 6 presents the NMSE of range and velocity versus SNR_b , and we can get the following conclusions:

- We can see that the dashed line of the same color is higher than the solid line, which indicates that an increase in the number of targets leads to an increase in NMSE of range

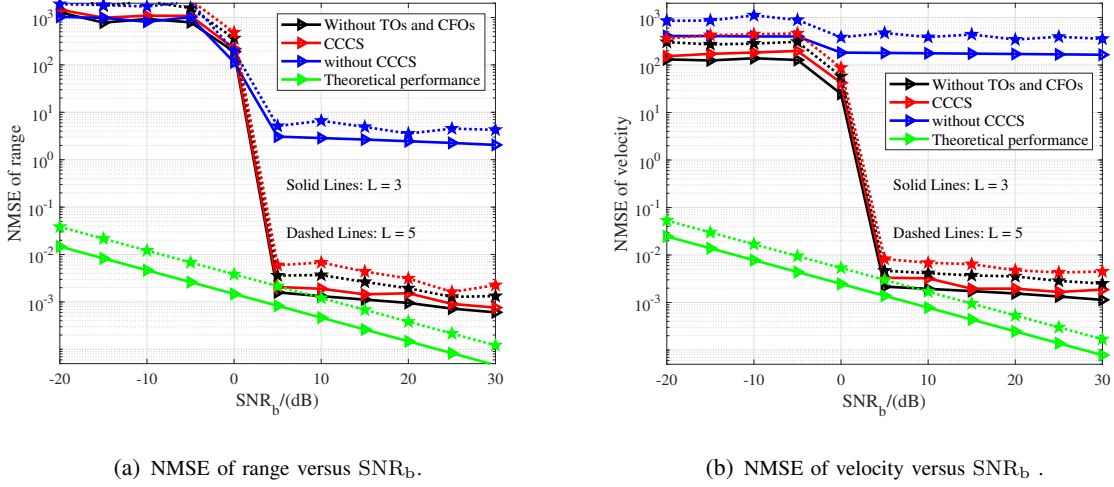
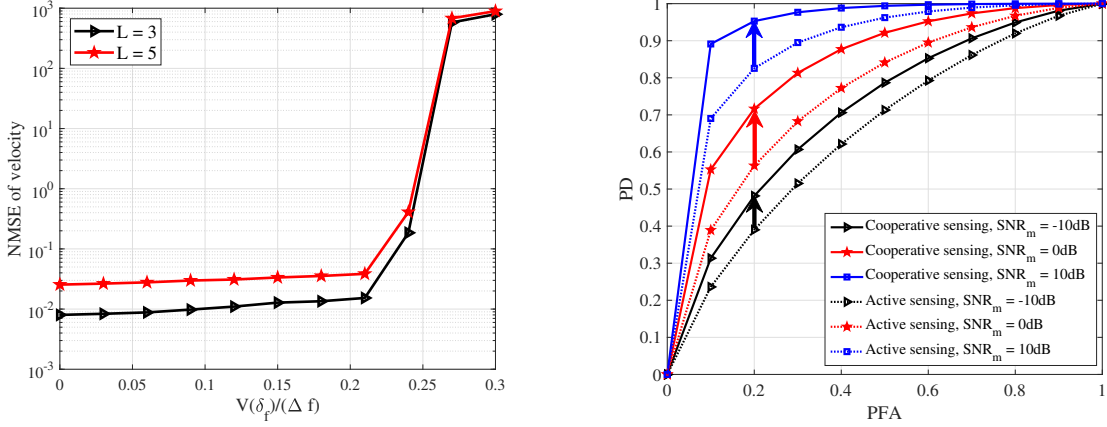


Fig. 6: NMSE of range and velocity versus SNR_b with $E(\delta_\tau) = 100$ ns, $V(\delta_\tau) = 100$, $E(\delta_f) = 0.2 \Delta f$ and $V(\delta_f) = 0.01$.

and velocity and a consequent decrease in estimation accuracy.

- We can see that the red line is well below the blue line and close to the black line, which means that CCCS can improve the passive sensing performance of range and velocity estimation under TOs and CFOs, close to the performance under perfect case, i.e., without TOs and CFOs.
- The green line in Fig. 6(a) denotes the theoretical performance of range estimation, which can be deduced by the standard deviation of Cramér–Rao bound, $\frac{\Delta R}{\sqrt{(2\text{SNR}_b)}}$ [51], with $\Delta R = \frac{c}{2B}$ being the ranging resolution. The green line in Fig. 6(b) denotes the theoretical performance of velocity estimation, which can be deduced by the standard deviation of Cramér–Rao bound, $\frac{\Delta V}{\sqrt{(2\text{SNR}_b)}}$, with $\Delta V = \frac{c}{2TMf_c2}$ being the velocity resolution. We can see that the red and black solid line is close to the green solid line when $\text{SNR}_b = 5$ dB, the sensing performance of range and velocity estimation by CCCS is close to the theoretical performance when $\text{SNR}_b = 5$ dB.

According to Fig. 4(d) and the analysis mentioned in Section III-C2, the variance of CFOs $V(\delta_f)$ results in that the Doppler spread on different OFDM symbols m is variable, which in turn affects the accuracy of DFT for estimating $\Delta f_{D,l} + \delta_f(m)$, further affects the performance of CCCS for mitigating CFOs, ultimately resulting in lower velocity estimation accuracy. Recognizing this fact, we simulate the NMSE of velocity versus $V(\delta_f)$, as shown in Fig. 7(a). We



(a) NMSE of velocity versus $V(\delta_f)$ with $\text{SNR}_b = 10$ dB, $E(\delta_f) = 0.2 \Delta f$, $E(\delta_\tau) = 100$ ns and $V(\delta_\tau) = 100$.

(b) ROC for different type sensing with $\text{SNR}_r = 0$ dB .

Fig. 7: NMSE of velocity and ROC

can see that the performance of CCCS for mitigating CFOs is relatively great when $V(\delta_f)$ is smaller than 0.25, which can be obtained by ordinary frequency sources [26]–[28].

2) *ROC of cooperative sensing*: In terms of target detection, the receiver operating characteristic (ROC) is an important metric, which denotes the relationship between the probability of detection (PD) and the probability of false alarm (PFA). Without loss of generality, assuming that $\text{SNR}_r = 0$ dB and Neyman-Pearson test principle is adopted [52]. As shown in Fig. 7(b), the ROC of cooperative sensing is higher than that of active sensing under the same SNR, which indicates that cooperative sensing can improve the target detection performance of active sensing to a certain extent.

C. AoA Estimation

Fig. 8(a) shows the root mean square error (RMSE) of the AoA estimation with variable SNR, which can be expressed as

$$\Gamma_A = \sqrt{\frac{1}{L} \sum_{l=0}^{L-1} |\Omega_{e,l} - \Omega_{r,l}|^2} \quad , \quad (45)$$

where $\Omega_{r,l}$ and $\Omega_{e,l}$ are the actual and estimated AoA of targets, respectively. We compare the proposed low complexity AoA estimation algorithm, i.e., Algorithm 3, with the FRFT from [29], the H-ESPRIT and H-MUSIC method from [13], and the TSF-MUSIC method from [12].

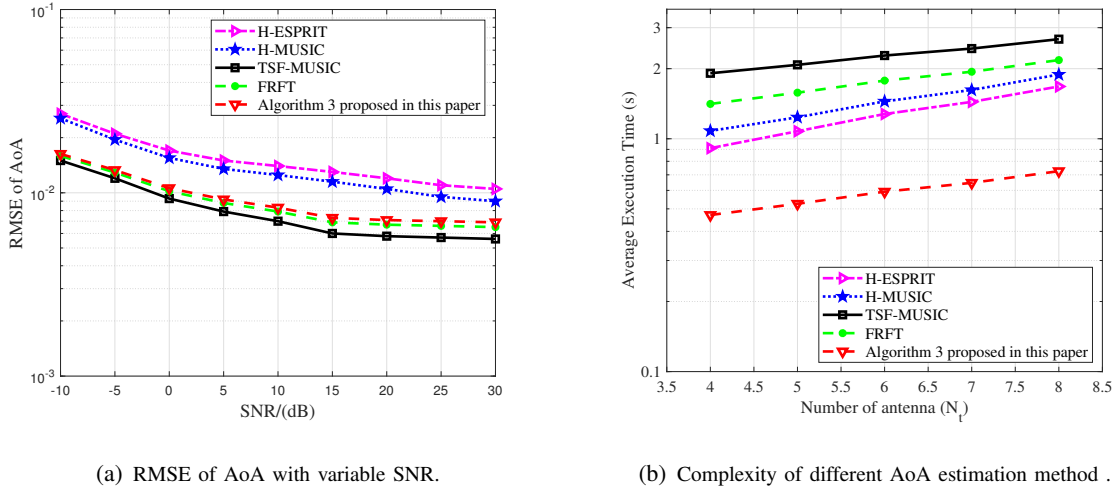


Fig. 8: RMSE of AoA with variable SNR and Complexity of different AoA estimation method.

- The fractional index of FRFT is set as $N_f = 10$, the uncertainty range of CAE is set as $\Omega = \frac{\pi}{3}$.
- The setup of MUSIC is the same as that in TSF-MUSIC method [12].

According to Fig. 8(a), RMSE of AoA, Γ_A is close to that of FRFT, which is lower than that of H-ESPRIT and H-MUSIC [13], but little higher than that of TSF-MUSIC [12], which means that the AoA estimation performance of Algorithm 3 is close to FRFT [29]. In Fig. 8(b), we explore the complexity of different methods by the average execution time, which reflects the average time to complete AoA estimation for different methods. We can see that the red line is much lower than other lines, which means that the complexity of Algorithm 3 is much lower than other algorithms. Therefore, simulation results show that Algorithm 3 can achieve relatively high-performance AoA estimation, close to FRFT, at a low complexity, much lower than FRFT.

VI. CONCLUSION

In this paper, we propose a cooperation based joint active and passive sensing scheme to improve the sensing performance in PMN. To overcome the clock asynchronicity problem in passive sensing, which is caused by the spatially separated asynchronous transceivers, we propose the CCCS based algorithm that mitigates TOs and CFOs by correlating active and passive sensing information. Compared with most existing algorithms, the CCCS based algorithm is

more widely applicable because it does not require the existence of LOS propagation paths between transceivers. Moreover, we propose a low complexity algorithm that adopts coarse and fine precision iterative estimation to achieve high-accuracy AoA estimation with low complexity. Finally, we analyze and simulate the performance improvement of the cooperation based joint active and passive sensing in delay and Doppler spread estimation. The simulation results verify the CCCS based algorithm and the performance improvement of cooperative sensing.

APPENDIX A

CCCS FOR MULTIPLE TARGETS

According to (20) and (22), the promotion from $D_R(n, k)$ to $D_R(n)$ can be derived as

$$w_D = \frac{D_R(n)}{D_R(n, k)} = N_t \quad . \quad (46)$$

According to (21) and (23), the promotion from $I_R(n, k)$ to $I_R(n)$ can be derived as

$$w_I = \frac{I_R(n)}{I_R(n, k)} = \sum_{k=0}^{\rightarrow N_t-1} e^{jk(\Omega_{l_2}-\Omega_{l_1})} \quad , \quad (47)$$

where $l_1 \neq l_2$, then Ω_{l_2} is not equal to Ω_{l_1} in most cases. Then,

$$w_I = \sum_{k=0}^{\rightarrow N_t-1} e^{jk(\Omega_{l_2}-\Omega_{l_1})} < N_t. \quad (48)$$

Therefore, $D_R(n, k)$ can be enhanced by calculate the vector sum of $\beta_R(n, k)$ on the N_t antennas.

REFERENCES

- [1] J. A. Zhang, A. Cantoni, X. Huang, Y. J. Guo, and R. W. Heath, "Framework for an innovative perceptive mobile network using joint communication and sensing," in *2017 IEEE 85th Vehicular Technology Conference (VTC Spring)*, Sydney, NSW, Australia, 2017, pp. 1–5.
- [2] M. L. Rahman, J. A. Zhang, X. Huang, Y. J. Guo, and R. W. Heath, "Framework for a perceptive mobile network using joint communication and radar sensing," *IEEE Transactions on Aerospace and Electronic Systems*, vol. 56, no. 3, pp. 1926–1941, June. 2020.
- [3] A. Zhang, M. L. Rahman, X. Huang, Y. J. Guo, S. Chen, and R. W. Heath, "Perceptive mobile networks: Cellular networks with radio vision via joint communication and radar sensing," *IEEE Vehicular Technology Magazine*, vol. 16, no. 2, pp. 20–30, June. 2021.
- [4] J. A. Zhang, M. L. Rahman, K. Wu, X. Huang, Y. J. Guo, S. Chen, and J. Yuan, "Enabling joint communication and radar sensing in mobile networks : A survey," *IEEE Communications Surveys & Tutorials*, vol. 24, no. 1, pp. 306–345, Firstquarter. 2022.
- [5] W. Jiang, A. Wang, Z. Wei, M. Lai, C. Pan, Z. Feng, and J. Liu, "Improve sensing and communication performance of uav via integrated sensing and communication," in *2021 IEEE 21st International Conference on Communication Technology (ICCT)*, Tianjin, China, 2021, pp. 644–648.

- [6] W. Jiang, Z. Wei, B. Li, Z. Feng, and Z. Fang, "Improve radar sensing performance of multiple roadside units cooperation via space registration," *IEEE Transactions on Vehicular Technology*, vol. 71, no. 10, pp. 10975–10990, Oct. 2022.
- [7] J. Yang, C.-K. Wen, and S. Jin, "Hybrid active and passive sensing for SLAM in wireless communication systems," *IEEE Journal on Selected Areas in Communications*, vol. 40, no. 7, pp. 2146–2163, 2022.
- [8] F. Alam, N. Faulkner, and B. Parr, "Device-free localization: A review of Non-RF techniques for unobtrusive indoor positioning," *IEEE Internet of Things Journal*, vol. 8, no. 6, pp. 4228–4249, Mar. 2021.
- [9] M. Dalla Mura, S. Prasad, F. Pacifici, P. Gamba, J. Chanussot, and J. A. Benediktsson, "Challenges and opportunities of multimodality and data fusion in remote sensing," *Proceedings of the IEEE*, vol. 103, no. 9, pp. 1585–1601, Sep. 2015.
- [10] R. Zhang, X. Jing, S. Wu, C. Jiang, J. Mu, and F. R. Yu, "Device-free wireless sensing for human detection: The deep learning perspective," *IEEE Internet of Things Journal*, vol. 8, no. 4, pp. 2517–2539, Feb. 2021.
- [11] J. A. Zhang, F. Liu, C. Masouros, R. W. Heath, Z. Feng, L. Zheng, and A. Petropulu, "An overview of signal processing techniques for joint communication and radar sensing," *IEEE Journal of Selected Topics in Signal Processing*, vol. 15, no. 6, pp. 1295–1315, Nov. 2021.
- [12] Z. Ni, J. A. Zhang, X. Huang, K. Yang, and J. Yuan, "Uplink sensing in perceptive mobile networks with asynchronous transceivers," *IEEE Transactions on Signal Processing*, vol. 69, pp. 1287–1300, 2021.
- [13] S. Chuang, W. Wu, and Y. Liu, "High-resolution AoA estimation for hybrid antenna arrays," *IEEE Transactions on Antennas and Propagation*, vol. 63, no. 7, pp. 2955–2968, July. 2015.
- [14] Z. Ni, J. A. Zhang, K. Yang, F. Gao, and J. An, "Estimation of multiple angle-of-arrivals with localized hybrid subarrays for millimeter wave systems," *IEEE Transactions on Communications*, vol. 68, no. 3, pp. 1897–1910, Mar. 2020.
- [15] Y. Peng, Y. Li, and P. Wang, "An enhanced channel estimation method for millimeter wave systems with massive antenna arrays," *IEEE Communications Letters*, vol. 19, no. 9, pp. 1592–1595, Sep. 2015.
- [16] P. Muneer and S. M. Sameer, "Joint ML estimation of CFO and channel, and a low complexity turbo equalization technique for high mobility OFDMA uplinks," *IEEE Transactions on Wireless Communications*, vol. 14, no. 7, pp. 3642–3654, July. 2015.
- [17] H. Chen, J. Hua, F. Li, F. Chen, and D. Wang, "Interference analysis in the asynchronous f-OFDM systems," *IEEE Transactions on Communications*, vol. 67, no. 5, pp. 3580–3596, May. 2019.
- [18] A. M. Hamza, J. W. Mark, and E. A. Sourour, "Interference analysis and mitigation for time-asynchronous OFDM CoMP systems," *IEEE Transactions on Wireless Communications*, vol. 17, no. 7, pp. 4780–4791, July. 2018.
- [19] C. Sexton, Q. Bodinier, A. Farhang, N. Marchetti, F. Bader, and L. A. DaSilva, "Enabling asynchronous machine-type D2D communication using multiple waveforms in 5G," *IEEE Internet of Things Journal*, vol. 5, no. 2, pp. 1307–1322, April. 2018.
- [20] Y. Jiang, Y. Wang, P. Cao, M. Safari, J. Thompson, and H. Haas, "Robust and low-complexity timing synchronization for DCO-OFDM LiFi systems," *IEEE Journal on Selected Areas in Communications*, vol. 36, no. 1, pp. 53–65, Jan. 2018.
- [21] J. A. Zhang, K. Wu, X. Huang, Y. J. Guo, D. Zhang, and R. W. Heath, "Integration of radar sensing into communications with asynchronous transceivers," *IEEE Communications Magazine*, vol. 60, no. 11, pp. 106–112, Nov. 2022.
- [22] X. Li, D. Zhang, Q. Lv, J. Xiong, S. Li, Y. Zhang, and H. Mei, "Indotrack: Device-free indoor human tracking with commodity Wi-Fi," *Proceedings of the ACM on Interactive, Mobile, Wearable and Ubiquitous Technologies*, vol. 1, pp. 1–22, Sep. 2017. [Online]. Available: <https://doi.org/10.1145/3130940>
- [23] K. Qian, C. Wu, Y. Zhang, G. Zhang, Z. Yang, and Y. Liu, "Widar2.0: Passive human tracking with a single Wi-Fi link," in *Proceedings of the 16th Annual International Conference on Mobile Systems, Applications, and Services*, ser. MobiSys '18. New York, NY, USA: Association for Computing Machinery, June. 2018, p. 350–361. [Online]. Available: <https://doi.org/10.1145/3210240.3210314>

- [24] D. Garmatyuk, P. Giza, N. Condict, and S. Mudaliar, "Randomized OFDM waveforms for simultaneous radar operation and asynchronous covert communications," in *2018 IEEE Radar Conference (RadarConf18)*, Oklahoma City, OK, USA, 2018, pp. 0975–0980.
- [25] C. Laoudias, A. Moreira, S. Kim, S. Lee, L. Wirola, and C. Fischione, "A survey of enabling technologies for network localization, tracking, and navigation," *IEEE Communications Surveys & Tutorials*, vol. 20, no. 4, pp. 3607–3644, July. 2018.
- [26] L. Romano, A. Bonfanti, S. Levantino, C. Samori, and A. Lacaita, "5-GHz oscillator array with reduced flicker up-conversion in 0.13- μm CMOS," *IEEE Journal of Solid-State Circuits*, vol. 41, no. 11, pp. 2457–2467, Nov. 2006.
- [27] C. Li and J. Lin, "A 1–9 GHz linear-wide-tuning-range quadrature ring oscillator in 130 nm CMOS for non-contact vital sign radar application," *IEEE Microwave and Wireless Components Letters*, vol. 20, no. 1, pp. 34–36, Jan. 2010.
- [28] F. Z. Merli, X. Wang, and G. M. Vitetta, "A bayesian multiuser detection algorithm for MIMO-ODFM systems affected by multipath fading, carrier frequency offset, and phase noise," *IEEE Journal on Selected Areas in Communications*, vol. 26, no. 3, pp. 506–516, April. 2008.
- [29] Z. Wei, H. Qu, W. Jiang, K. Han, H. Wu, and Z. Feng, "Iterative signal processing for integrated sensing and communication systems," *IEEE Transactions on Green Communications and Networking*, vol. 7, no. 1, pp. 401–412, Mar. 2023.
- [30] X. Chen, Z. Feng, Z. Wei, P. Zhang, and X. Yuan, "Code-division OFDM joint communication and sensing system for 6G machine-type communication," *IEEE Internet of Things Journal*, vol. 8, no. 15, pp. 12 093–12 105, Aug. 2021.
- [31] J. A. Zhang, X. Huang, Y. J. Guo, J. Yuan, and R. W. Heath, "Multibeam for joint communication and radar sensing using steerable analog antenna arrays," *IEEE Transactions on Vehicular Technology*, vol. 68, no. 1, pp. 671–685, Jan. 2019.
- [32] F. Liu, C. Masouros, A. P. Petropulu, H. Griffiths, and L. Hanzo, "Joint radar and communication design: Applications, state-of-the-art, and the road ahead," *IEEE Transactions on Communications*, vol. 68, no. 6, pp. 3834–3862, June. 2020.
- [33] Q. Zhang, X. Wang, Z. Li, and Z. Wei, "Design and performance evaluation of joint sensing and communication integrated system for 5G mmwave enabled CAVs," *IEEE Journal of Selected Topics in Signal Processing*, vol. 15, no. 6, pp. 1500–1514, Nov. 2021.
- [34] Z. Feng, Z. Fang, Z. Wei, X. Chen, Z. Quan, and D. Ji, "Joint radar and communication: A survey," *China Communications*, vol. 17, no. 1, pp. 1–27, Jan. 2020.
- [35] L. Liu, Y. Zhou, A. V. Vasilakos, L. Tian, and J. Shi, "Time-domain intercell interference coordination for LTE-based heterogeneous small cell networks and optimized designs for 5G: A survey," *Sci. China Informat. Sci.*, vol. 62, pp. 1–28, Feb. 2019.
- [36] 3GPP, "Summary of release 15 work items," *3rd Generation Partnership Project (3GPP)*, TR 21.915 Version 1.1.0 Release 15, 2018.
- [37] S. D. Liyanaarachchi, T. Riihonen, C. B. Barneto, and M. Valkama, "Optimized waveforms for 5G–6G communication with sensing: Theory, simulations and experiments," *IEEE Transactions on Wireless Communications*, vol. 20, no. 12, pp. 8301–8315, Dec. 2021.
- [38] C. Sturm, T. Zwick, W. Wiesbeck, and M. Braun, "Performance verification of symbol-based OFDM radar processing," in *2010 IEEE Radar Conference (IRC)*, Arlington, VA, USA, 2010, pp. 60–63.
- [39] Y. Liu, G. Liao, J. Xu, Z. Yang, and Y. Zhang, "Adaptive OFDM integrated radar and communications waveform design based on information theory," *IEEE Communications Letters*, vol. 21, no. 10, pp. 2174–2177, Oct. 2017.
- [40] X. Tian, T. Zhang, Q. Zhang, and Z. Song, "Waveform design and processing in OFDM based radar-communication integrated systems," in *2017 IEEE/CIC International Conference on Communications in China (ICCC)*, Qingdao, 2017, pp. 1–6.

- [41] M. Bică and V. Koivunen, "Generalized multicarrier radar: Models and performance," *IEEE Transactions on Signal Processing*, vol. 64, no. 17, pp. 4389–4402, Sept. 2016.
- [42] T. Cui, F. Gao, A. Nallanathan, H. Lin, and C. Tellambura, "Iterative demodulation and decoding algorithm for 3GPP/LTE-A MIMO-OFDM using distribution approximation," *IEEE Transactions on Wireless Communications*, vol. 17, no. 2, pp. 1331–1342, Feb. 2018.
- [43] W. Zhang, F. Gao, and Q. Yin, "Blind channel estimation for MIMO-OFDM systems with low order signal constellation," *IEEE Communications Letters*, vol. 19, no. 3, pp. 499–502, Mar. 2015.
- [44] Y. Lin, S. Jin, M. Matthaiou, and X. You, "Tensor-based algebraic channel estimation for hybrid ired-assisted mimo-ofdm," *IEEE Transactions on Wireless Communications*, vol. 20, no. 6, pp. 3770–3784, June. 2021.
- [45] H. He, C.-K. Wen, and S. Jin, "Bayesian optimal data detector for hybrid mmwave MIMO-OFDM systems with low-resolution ADCs," *IEEE Journal of Selected Topics in Signal Processing*, vol. 12, no. 3, pp. 469–483, June. 2018.
- [46] B. Lu, G. Yue, and X. Wang, "Performance analysis and design optimization of LDPC-coded MIMO OFDM systems," *IEEE Transactions on Signal Processing*, vol. 52, no. 2, pp. 348–361, Feb. 2004.
- [47] A. Almradi and K. A. Hamdi, "Spectral efficiency of OFDM systems with random residual CFO," *IEEE Transactions on Communications*, vol. 63, no. 7, pp. 2580–2590, July. 2015.
- [48] C. Sturm and W. Wiesbeck, "Waveform design and signal processing aspects for fusion of wireless communications and radar sensing," *Proceedings of the IEEE*, vol. 99, no. 7, pp. 1236–1259, July. 2011.
- [49] K. Wu, J. A. Zhang, X. Huang, and Y. J. Guo, "Integrating low-complexity and flexible sensing into communication systems," *IEEE Journal on Selected Areas in Communications*, vol. 40, no. 6, pp. 1873–1889, June 2022.
- [50] G. T. S. 38.913, "Study on scenarios and requirements for next generation access technologies, Rel 14," 2020.
- [51] F. Zhu, "A survey of vehicular radar communication systems (in Chinese)," *ZTE Communications Technology*, vol. 24, no. 3, pp. 32–38, June 2018.
- [52] H. L. Van Trees and K. L. Bell, "Excerpts from Part I of detection, estimation, and modulation theory," *Bayesian Bounds for Parameter Estimation and Nonlinear Filtering/Tracking*, pp. 89–109, IEEE. 2007.